Structural properties of Bi/Au(110)

Egzona Neziri, Wei Zhang, Alexander Smogunov, Andrew Mayne, Abdelkader Kara, Yannick Dappe, Hamid Oughaddou

STRUCTURAL AND ELECTRONIC PROPERTIES OF Bi/Au(110)

Egzona Neziri[1], Wei Zhang[1], Alexander Smogunov[2], Andrew J. Mayne[1], Abdelkader Kara[3,4], Yannick J. Dappe[2], and Hamid Oughaddou[1,5]

[1]*Université Paris-Saclay, CNRS, Institut des Sciences Moléculaires d'Orsay, 91405 Orsay, France Gif-sur-Yvette Cedex, France*

[2]*Université Paris-Saclay, CNRS, CEA, Service de Physique de l'Etat Condensé, 91191 Gif-sur-Yvette, France*

[3]*Department of Physics, University of Central Florida, Orlando, FL 32816, USA*

[4]*IRMC, Imam Abdulrahman Bin Faisal University, Dammam, Saudi Arabia*

[5]*Département de physique, CY Cergy Paris Université, F-95031 Cergy-Pontoise Cedex, France*

Atomically thin bismuth films (2D Bi) are becoming a promising research area due to their wide variety of applications as for example in spintronics, electronic and optoelectronic devices. Here we report on the structural and electronic properties of Bi on Au(110), explored by low-energy electron diffraction (LEED), scanning tunneling microscopy (STM) and density functional theory (DFT) calculations. Below the monolayer Bi coverage, various reconstructions are observed. We focus here on Bi/Au(110)-c(2x2) reconstruction (at 0.5ML) and Bi/Au(110)-(3x3) structure (at 0.66ML) and propose models for both structures based on STM measurements, and further confirmed by DFT calculations.

The discovery of graphene's fascinating properties [1] has led to numerous theoretical and experimental studies of novel two-dimensional (2D) materials [2]. In particular, there is an important focus on monoelemental 2D materials beyond graphene, like silicone [3-5], germanene [6], phosphorene [7,8] (Nature Communications, 2021, 12(1), 5160)) and stanine [9]. The reason is that 2D materials can show interesting properties when compared to their bulk form, e.g. higher charge carrier mobility [10], transparency and flexibility [11], thickness-dependent band gaps [12-13].

In this context, 2D bismuth has been highlighted recently for its unique advantages and superior properties. Bulk bismuth is a semimetal characterized by an indirect band overlap of 30-40 meV [14-17].

If the thickness is reduced down to the monolayer, a transition from semimetal to semiconductor is observed[18,19]. Moreover, the strong Bi spin-orbit coupling (SOC) allows the generation of spin-polarized electrons without the need of a magnetic field, enabling possible applications in future spintronic devices[20]. Owing to this strong SOC, Rashba splitting surface states have been observed in bulk and thin film B[20,21]. The high carrier mobility of bulk and Bi thin film has also opened new possible applications in ultrafast transistors[22]. On the other hand, it was predicted theoretically that 2D Bi could host 2D topological Insulator (TI) states[23-24]. Various groups have already explored 2D Bi for practical applications. For example, sodium-ion batteries are an emerging alternative in the energy storage systems. In these systems, 2D Bi

(few layers of bismuth nanosheets) is seen as a possible candidate for the anode material, in general due to the enhanced gaps between the nanosheets, therefore, leading to the penetration of sodium ions within the crystal structure without facing pulverization problems[25]. Yang *et al.* proved that free-standing single layer bismuth can also be used for carbon dioxide reduction reaction[26]. They experimentally proved that 2D Bi could selectively catalyze the formation of formic acid from CO_2 and interpret it as an effect of higher surface density of active sites, higher electronic conductivity and higher structural stability of 2D Bi. Lu *et al.*[27] showed that Bi single layer could be considered as a new kind of optical Kerr and saturable absorber material, characterized by enhanced stability. This research could open new ways for designing 2D bismuth-based photonics.

An important work was done by Reis *et al.*[28] regarding room-temperature 2D TI based on 2D bismuth. Moreover, high nonlinear optical properties and small band gap are some of the properties that make 2D Bi suitable for promising applications [29,30]. However, an important difficulty remains in obtaining high-quality 2D bismuth films. For instance, 2D Bi films growth has been achieved by various methods including, liquid exfoliation [31,32], hot-pressing [33], physical vapor deposited (PVD) [34], pulsed laser deposition (PLD)[35], MBE[28] and wet chemical methods[36]. Unlike other 2D materials, for example silicene and phosphorene layers, that require a substrate to support them, 2D Bi is expected to be stable at room temperature and under standard conditions[28].

Theoretically, there exist three stable phases of 2D bismuth or bismuthene, namely α-, β-, and ζ-phases[37]. Among these phases, only α- and β-phase of bismuthene have been experimentally obtained. Figure 1a shows the top and side views of β-phase bismuthene, exhibiting a buckled rhombohedral structure[38]. Meanwhile, Figure 1b shows the views of α-phase bismuthene exhibiting a puckered black-phosphorous-like structure[39].

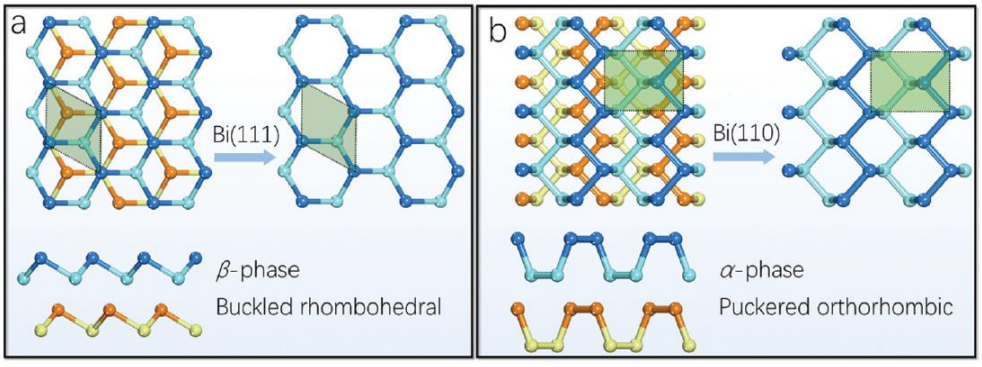

Figure 1: Schematic illustration of a) top and side views of β-phase bismuthene. b) Top and side views of α-phase bismuthene[40].

However, these phases might be modified and new phases might arise through Bi growth on specific substrates, and very little studies have been performed until now. For example, structural and electronic properties of Bi/Au(110) system have only been studied in 2013 by Crepaldi *et al.*[41]. They showed that at a coverage of ~ 1 ML, a 1x4 reconstruction appears. Meanwhile, at lower coverage (~ 0.875 ML) they observed a 1x8 reconstruction. However, they did not investigate other surfaces.

Bi growth on the Ag(111) surface has been studied by other groups [42-43]. Different ordered structures were observed. At low coverage (<1 ML) 2D Bi array structures were obtained while at higher coverage (>1 ML) the thicker Bi films grew with a lattice constant close to that of the bulk bi (110) surface [44].

The aim of this work is the synthesis of a 2D atomically thin Bi film on Au(110) surface using molecular beam epitaxy method (MBE). We report on the structural evolution of the film as a function of Bi coverage, using LEED, STM and STS techniques. A variety of reconstructions is observed below one monolayer (1ML) of Bi deposition. We focus on the Bi/Au(110)-c(2x2) structure (~ 0.5ML) and on Bi/Au(110)-(3x3) structure (~ 0.66ML). Models are proposed for both structures, for which DFT calculated STM images match those observed experimentally.

The ultrahigh vacuum apparatus, where the experiments are performed, is equipped with the standard tools for surface preparation and characterization. An ion gun is used for surface cleaning, Low Energy Electron Diffraction (LEED) for crystallographic structure, an Auger electron spectrometer (AES) for chemical surface analysis, and an Omicron scanning tunneling microscope (LT-STM) for atomic scale surface characterization at 77 K. Commercial Au(110) crystals with 99.999% purity were used. The Au(110) substrate was cleaned by several sputtering cycles (2 keV Ar+ ions, $P = 5 \times 10^{-6}$ mbar) followed by annealing at 500 °C for 1h. A cell loaded with bismuth was used to grow 2D Bi on Au(110) substrate. The Au(110) surface was held at room temperature during the deposition meanwhile surface structure and thickness, and chemical structure were systematically controlled by AES and LEED. All STM experiments were carried out at 77 K with a base pressure during the experiments of $<3.0 \times 10^{-10}$ mbar.

We have utilized the Vienna Ab into Simulation Package (VASP) version 5.4.4.[45-47], which uses the projector augmented wave (PAW) method [48,49] to study the adsorption of Bi on Au(110). To model the exchange-correlation interaction we have employed the optB88-vdW functional [50]. This particular functional includes a nonlocal implementation of the correlation energy term which incorporates self-consistently the long-range van der Waals (vdW) interactions. Several previous studies demonstrated the importance of the vdW interactions (including the use of optB88) to a large set of systems [51-55], including organic molecules on transition metal substrates. To model our surfaces, we created a 5-layer slab with

each layer containing either 4 or 9 atoms, corresponding to the 2x3 and 3x3 surface reconstructions, respectively. To separate the slabs, 23 Å of vacuum is placed between them. We used a lattice constant of 4.178 Å. To achieve structural relaxation, the conjugate gradient method is applied, with a force criterion limit set to 0.02 eV/Å, the plane wave energy cutoff is at 400 eV, and the Brillouin zone is sampled using a 12x12x1 and 8x8x1 k-point mesh for the 2x2 and 3x3 surface reconstructions, respectively. STM images were calculated using charge densities following the Tersoff and Hamann scheme[55], as implemented in P4VASP [56].

During bismuth deposition, the Au(110) substrate was kept at room temperature. After Bi adsorption at a coverage below 1 ML, the (2x1) Au structure undergoes several reconstructions. In this work we study two phases which we identify as: Bi/Au(110)-c(2x2) and Bi/Au(110)-(3x3). Deposition of 0.5 ML of Bi gives rise to the LEED pattern shown in Figure 2b. If compared to clean Au(110) substrate in Figure 2a, the diffraction spots corresponding to the (2x2) of Au(110) structure disappear and sharp spots corresponding to the (1x1) Au structure are observed. Moreover, extra spots appear indicating the formation of an ordered Bi structure on the surface. This LEED pattern reveals a c(2x2) superstructure with respect to Au(110) which remains stable even after annealing up to 350˚C. After deposition of 0.66 ML of Bi, the LEED pattern evolves and extra spots appear, revealing a new reconstruction. We assign it as a (3x3) superstructure with respect to Au(110), seen in Figure 2c.

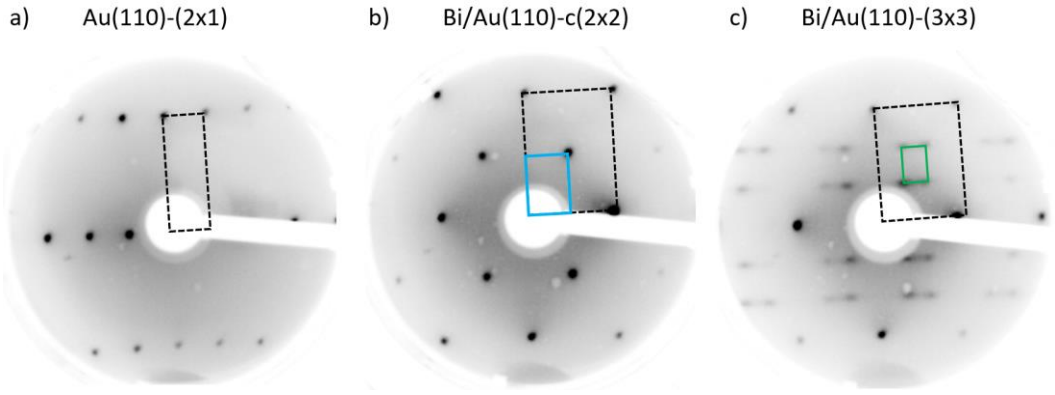

Figure 2. LEED pattern of a) clean (2x1) Au surface; b) Bi/Au(110)-c(2x2) surface (~ 0.5 ML Bi deposition) c) Bi/Au(110)-(3x3) surface (~ 0.66 ML Bi deposition). The black and blue dashed rectangles represent the (2x1) and (1x1) Au(110) unit cell. The red and green ones show the unit cell of c(2x2) and (3x3) superstructures after Bi deposition at RT. The energy value is indicated for each measurement.

The STM images show the two different structural reconstructions of Bi deposited on Au(110) at room temperature. First, we discuss the Au(110)-Bi-c(2x2) structure obtained after deposition of ~ 0.5 ML of Bi. It is possible to notice significant changes when compared to clean Au(110) (Figure 3b). Centered (2x2) structure can be clearly seen at higher atomic resolution including 2 Bi atoms per unit cell (Figures 3a and

d). Line scans show the distance between Bi atoms in both directions, namely in blue an interatomic distance of 8 Å ~ 2 x 4.08 Å, and in green, an interatomic distance of 6 Å ~ 2 x 2.88 Å in agreement with the c(2x2) LEED pattern (Figure 2b). The surface seems relatively flat, despite some missing atoms and random defects (Figure 3a). The superstructure unit cell is aligned in same direction as Au(110) shown in Figures 3b and d.

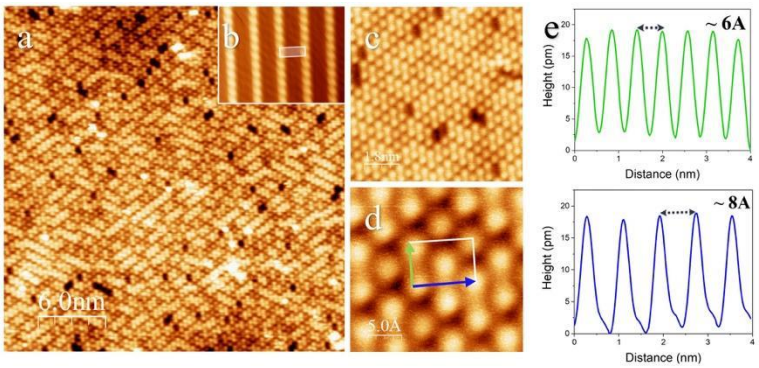

Figure 3. STM image of bismuth deposited on Au(110) for 27 minutes at room temperature; a) Large scale STM image (41x41 nm^2, V_b=0.01 V, I_t=1.3 nA);b) Clean Au(110) structure (9.8x9.8 nm^2, V_b=0.3 V, I_t=3.7 nA); c) Higher resolution image of reconstructed surface (10x10 nm^2, V_b=0.6 V, I_t=1 nA); d) Higher resolution image showing c(2x2) superstructure (3x3 nm^2, V_b=0.6 V, I_t=1 nA). The c(2x2) unit cell is highlighted by the white rectangle; e) Line scans for each direction in green and blue.

After a Bi deposition of ~ 0.66 ML the c(2x2) pattern disappears and a new LEED pattern appears. The unit cell of this new structure corresponds to the matrix $\begin{bmatrix} -1 & 2 \\ -1 & 1 \end{bmatrix}$ with two domains (Figure 2c). This LEED pattern can also be represented by a (3x3) unit cell with systematic extinction spots given by indices (n,0) and (0,n) (see Figure 2c).

In the STM images shown in Figure 4, we observe Bi dimers. In the larger scale image (Figure 4a) it first appears that the surface is separated in domains but at higher atomic resolution Figure 4c, and 4d we conclude that this is not the case. The unit cell is present in two different motifs with the same formation probability, arising from symmetry of the dimer motif with respect to the Au(110) substrate. On the atomically resolved STM image (Figure 4e) we plotted the reduced unit cell corresponding to the matrix $\begin{bmatrix} -1 & 2 \\ -1 & 1 \end{bmatrix}$ as well as the (3x3) unit cell.

Compared to the c(2x2) superstructure, the present structure has 6 Bi atoms per unit cell. In this case, the line scans show 12 Å ~ 3 x 4.08 Å (in blue) and 9 Å ~ 3 x 2.88 Å (in green) in good agreement with the (3x3) LEED pattern.

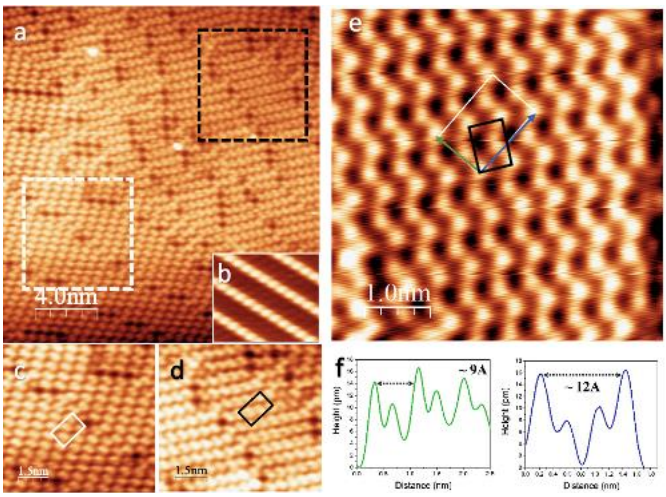

Figure 4. STM image of bismuth deposited on Au(110) for 32 minutes at room temperature. a) Large scale STM image (22x22 nm^2, V_b=0.02 V, I_t=2 nA); b) Clean Au(110) structure (9.8x9.8nm^2, V_b=0.3V, I_t=3.7nA); c) Zooming white dashed square; d) Zooming black dashed square; e) Higher resolution of (3x3) superstructure (5x5 nm^2, V_b=0.2 V, I_t=0.6 nA). The (3x3) unit cell is highlighted by a white rectangle while the matrix unit cell is in black (reduced one); f) Line scans from each direction in green and blue.

Let us recall that the Bi growth on Au(110) has already been investigated in aqueous conditions. Using the STM technique, the images revealed that the Bi atoms form an ordered structure showing Bi dimers similar to our results. However, the structure is different which can be due to the growth method used. Indeed, with a solution-based process it is difficult to control the deposition rate of Bi since it will depend on the solvation of the Bi ions and the dynamics of the electro-deposition at the 0.75V potential. The corresponding coverage of Bi is probably different from the case of the (3x3) structure [57].To support this experimental work, we further propose structural models for c(2x2) and (3x3) Bi reconstructions on Au(110). We consider a slab model of 5 Au(110) atomic layers terminated by a c(2x2) or a (3x3) Bi monolayer. The three upper layers are optimized meanwhile the bottom two layers are kept fixed. Note that we use here a non-reconstructed Au(110) surface. We found that Bi binds very strongly to the Au substrate with a binding energy of 2.26 eV/atom. Before adsorption of Bi on Au(110), the distance between the first and second layer was found to be contracted by about 13%, as compared to the distance between two adjacent layers in Au bulk. Upon Bi adsorption, this distance was found to revert to an expansion of about 3%, as compared to that in the bulk. The distance between the Bi layer and the top Au layer is found to be 1.37 Å.

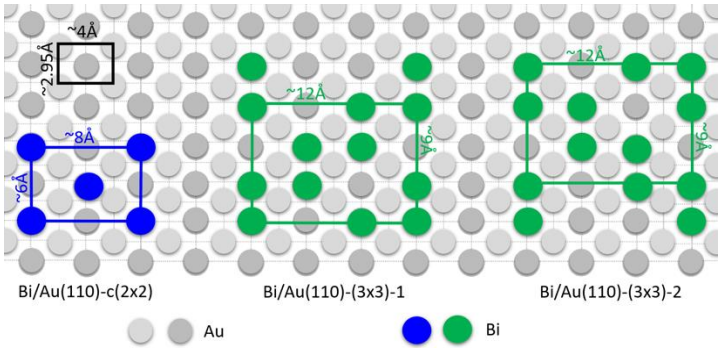

Figure 5 – Top view of proposed models of a) Bi/Au(110)-c(2x2) surface; b) Bi/Au(110)-(3x3) first motif; c) Bi/Au(110)-c(3x3) second motif. The c(2x2) unit cell is shown in blue, the (3x3) in green and Au (1x1) in black. Bi atoms and Au atoms are shown in blue/green and grey, respectively.

Using the calculated charge densities, we have considered the Tersoff and Hamann technique to determine STM images for both the Bi/Au(110)-c(2x2) and Bi/Au(110)-(3x3) reconstructions. In Figure 6, we show a comparison between calculated and observed STM images for Bi/Au(110)-c(2x2). As a result, we note the remarkable agreement between the two images. We also note that the image is formed by a repletion of a centered rectangle where corners and center are occupied by Bi atoms (see figure 5). Note that Au atoms are not seen here.

In Figure 7, we show a comparison between calculated and observed STM images for the Bi/Au(110)-(3x3) reconstruction. Again, here we note that the simulated STM image is in remarkable agreement with the STM image. The protrusions show the Bi dimers present in Figure 5.

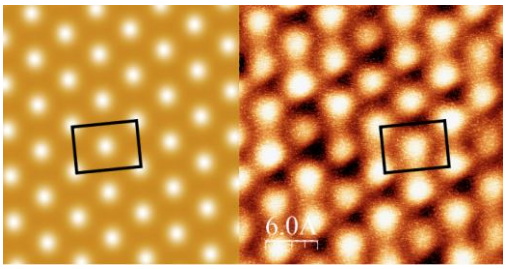

Figure 6: Calculated (left) and measured (right) STM images for Bi/Au(110)-c(2x2)

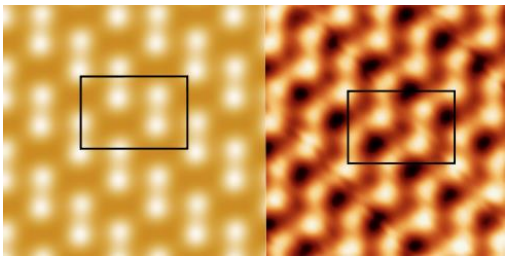

Figure 7: Calculated and measured STM images for Bi/Au(110)-(3x3)

Conclusion

In conclusion, we have used molecular beam epitaxy method to synthesize 2D bismuth ultrathin film on Au(110) substrate. We have characterized these films using LEED and AES at room temperature and as well as STM at 77K. The experimental measurements reveal two main reconstructions of Bi on Au(110). We assigned them as Bi/Au(110)-c(2x2) and Bi/Au(110)-(3x3). Both structures have never been studied before. The atomic and electronic structures of these reconstructions have been determined experimentally. 2D Bi has and will continue to attract attention due to its interesting electronic properties but also due to its wide variety of applications. Previous work has shown that theoretical calculations are essential for a complete understanding of the surface reconstructions formed during the fabrication of this 2D material. In order to obtain free-standing Bi layers, the growth of this Bi 2D film will need to be tested on other substrates. Regardless of the substrate, this material will show fascinating properties. It is safe to say that there will be more research opportunities regarding this 2D material and most probably such materials will lead to future technological advancements in electronics, sensing and energy-related devices.

Acknowledgements

We thank the French Ministry for Foreign Affaires for funding the Hubert Curien project “Bismuthene” n° 40769ZH. We thank S.A. Brown and T. Maerkl for helpful discussions on Bi deposition.

Conflict of Interest

There are no conflicts of interest to declare.

Notes and References

1 A. K. Geim, ‘Graphene: Status and Prospects’, *Science*, 2009, 324, 1530–1534, doi: 10.1126/science.1158877.

2 N. Antonatos, H. Ghodrati, and Z. Sofer, 'Elements beyond graphene: Current state and perspectives of elemental monolayer deposition by bottom-up approach', *Applied Materials Today*, 2020, 18, 100502, doi: 10.1016/j.apmt.2019.100502.

3. H. Enriquez et al., Atomic structure of the $(2\sqrt{3}\times2\sqrt{3})R30°$ of silicene on Ag(111) surface, *J. Phys.: Conf. Ser.* 2014, 491, 012004, doi: 10.1088/1742-6596/491/1/012004

4 H. Oughaddou, H. Enriquez, M.R. Tchalala, H. Yildirim, A.J. Mayne, A. Bendounan, G. Dujardin, M. Ait Ali, A. Kara, "Silicene: A promising new 2D material", *Prog. Surf. Sci.* 2015, 90, 1-46.

5 J. Zhao *et al.*, 'Rise of silicene: A competitive 2D material', *Progress in Materials Science*, 2016, 83, 24–151, doi: 10.1016/j.pmatsci.2016.04.001.

6 L. Li *et al.*, 'Buckled Germanene Formation on Pt(111)', *Advanced Materials*, 2014, 28, 4820–4824, 2014, doi: 10.1002/adma.201400909.

7 W. Zhang, H. Enriquez, Y. Tong, A. Bendounan, A. Kara, A. P. Seitsonen, A. J. Mayne, G. Dujardin and H. Oughaddou, "Epitaxial Synthesis of Blue Phosphorene", *Small*, 2018, **14**, 1804066.

8 W. Zhang, H. Enriquez, Y. Tong, A. J. Mayne, A. Bendounan, A. Smogunov, Y. J. Dappe, A. Kara, G. Dujardin and H. Oughaddou, "Flat epitaxial quasi-1D Phosphorene chains", *Nature Commun.* 2021, **12**, 5160-5165.

9 Zhu *et al.*, 'Epitaxial growth of two-dimensional stanene', *Nature Mater*, 2015, 10, 10, doi: 10.1038/nmat4384.

10 Li, L.; Yu, Y.; Ye, G. J.; Ge, Q.; Ou, X.; Wu, H.; Feng, D.; Chen, X. H.; Zhang, Y. Black Phosphorus Field-Effect Transistors. Nat. Nanotechnol. 2014, 9, 372–377.

11 Lee, G.-H.; Yu, Y.-J.; Cui, X.; Petrone, N.; Lee, C.-H.; Choi, M. S.; Lee, D.-Y.; Lee, C.; Yoo, W. J.; Watanabe, K.; Taniguchi, T.; Nuckolls, C.; Kim, P.; Hone, J. Flexible and Transparent MoS2 Field-Effect Transistors on Hexagonal Boron Nitride-Graphene Heterostructures. ACS Nano 2013, 7, 7931–7936. https://doi.org/10.1021/nn402954e.

12 Chaoliang Tan, Xiehong Cao, Xue-Jun Wu, Qiyuan He, Jian Yang, Xiao Zhang, Junze Chen, Wei Zhao, Shikui Han, Gwang-Hyeon Nam, Melinda Sindoro, and Hua Zhang, "Recent Advances in Ultrathin Two-Dimensional Nanomaterials", Chemical Reviews 2017, 117, 6225-6331. https://pubs.acs.org/doi/10.1021/acs.chemrev.6b00558.

13 G. Fiori, F. Bonaccorso, G. Iannaccone, T. Palacios, D. Neumaier, A. Seabaugh, S. K. Banerjee and L. Colombo, Electronics Based on Two-Dimensional Materials. Nat. Nanotechnol. 2014, 9, 768-779.

14 Behnia, K.; Balicas, L.; Kopelevich, Y. Signatures of Electron Fractionalization in Ultraquantum Bismuth. Science 2007, 317, 1729–1731. https://doi.org/10.1126/science.1146509.

15 Li, L.; Checkelsky, J. G.; Hor, Y. S.; Uher, C.; Hebard, A. F.; Cava, R. J.; Ong, N. P. Phase Transitions of Dirac Electrons in Bismuth. Science 2008, 321, 547–550. https://doi.org/10.1126/science.1158908.
16 Zhu, Z.; Collaudin, A.; Fauque, B.; Kang, W.; Behnia, K. Field-Induced Polarisation of Dirac Valleys in Bismuth. Nat. Phys. 2012, 8, 89–94. https://doi.org/10.1038/nphys2111.
17 Yang, Z.; Wu, Z.; Lyu, Y.; Hao, J. Centimeter-Scale Growth of Two-Dimensional Layered High-Mobility Bismuth Films by Pulsed Laser Deposition. InfoMat. 2019, 1, 98–107. https://doi.org/10.1002/inf2.12001.
18 Z. Zhu, A. Collaudin, B. Fauqué, W. Kang, and K. Behnia, 'Field-induced polarization of Dirac valleys in bismuth', *Nature Phys*, 2012, 8, 89–94, doi: 10.1038/nphys2111.
19 J.-T. Sun, H. Huang, S. L. Wong, H.-J. Gao, Y. P. Feng, and A. T. S. Wee, 'Energy-Gap Opening in a Bi(110) Nanoribbon Induced by Edge Reconstruction', *Phys. Rev. Lett.*, vol. 109, no. 24, p. 246804, Dec. 2012, doi: 10.1103/PhysRevLett.109.246804.
20 H. Du *et al.*, 'Surface Landau levels and spin states in bismuth (111) ultrathin films', *Nat Commun*, vol. 7, no. 1, Art. no. 1, Mar. 2016, doi: 10.1038/ncomms10814.
21 A. Takayama, T. Sato, S. Souma, T. Oguchi, and T. Takahashi, 'Tunable Spin Polarization in Bismuth Ultrathin Film on Si(111)', *Nano Lett.*, vol. 12, no. 4, pp. 1776–1779, Apr. 2012, doi: 10.1021/nl2035018.
22 Yu. M. Koroteev *et al.*, 'Strong Spin-Orbit Splitting on Bi Surfaces', *Phys. Rev. Lett.*, vol. 93, no. 4, p. 046403, Jul. 2004, doi: 10.1103/PhysRevLett.93.046403.
23 Y. Lu *et al.*, 'Topological Properties Determined by Atomic Buckling in Self-Assembled Ultrathin Bi(110)', *Nano Lett.*, vol. 15, no. 1, pp. 80–87, Jan. 2015, doi: 10.1021/nl502997v.
24 F. Schindler, Z. Wang, M. G. Vergniory, A. M. Cook, A. Murani, S. Sengupta, A. Yu. Kasumov, R. Deblock, S. Jeon, I. Drozdov, H. Bouchiat, S. Guéron, A. Yazdani, B. Andrei Bernevig and T. Neupert, *Nature Phys.* 2018, **14**, 918-924.
25 Y. Huang *et al.*, 'Ultrathin Bismuth Nanosheets for Stable Na-Ion Batteries: Clarification of Structure and Phase Transition by in Situ Observation', *Nano Lett.*, vol. 19, no. 2, pp. 1118–1123, Feb. 2019, doi: 10.1021/acs.nanolett.8b04417.
26 F. Yang *et al.*, 'Bismuthene for highly efficient carbon dioxide electro-reduction reaction', *Nat Commun*, vol. 11, no. 1, p. 1088, Dec. 2020, doi: 10.1038/s41467-020-14914-9.
27 L. Lu *et al.*, 'Few-layer Bismuthene: Sonochemical Exfoliation, Nonlinear Optics and Applications for Ultrafast Photonics with Enhanced Stability (Laser Photonics Rev. 12(1)/2018)', *Laser & Photonics Reviews*, vol. 12, no. 1, p. 1870012, Jan. 2018, doi: 10.1002/lpor.201870012.21
28 F. Reis *et al.*, 'Bismuthene on a SiC substrate: A candidate for a high-temperature quantum spin Hall material', *Science*, vol. 357, no. 6348, pp. 287–290, Jul. 2017, doi: 10.1126/science.aai8142.

29 J. D. Yao, J. M. Shao, and G. W. Yang, 'Ultra-broadband and high-responsive photodetectors based on bismuth film at room temperature', *Sci Rep*, vol. 5, no. 1, Art. no. 1, Jul. 2015, doi: 10.1038/srep12320.
30 L. Lu *et al.*, 'All-Optical Switching of Two Continuous Waves in Few Layer Bismuthene Based on Spatial Cross-Phase Modulation', *ACS Photonics*, vol. 4, no. 11, pp. 2852–2861, Nov. 2017, doi: 20.1021/acsphotonics.7b00849.
31 H. L. Chia, N. M. Latiff, R. Gusmão, Z. Sofer, and M. Pumera, 'Cytotoxicity of Shear Exfoliated Pnictogen (As, Sb, Bi) Nanosheets', *Chemistry – A European Journal*, vol. 25, no. 9, pp. 2242–2249, 2019, doi: 10.1002/chem.201804336.
32 N. Hussain *et al.*, 'Ultrathin Bi Nanosheets with Superior Photoluminescence', *Small*, vol. 13, no. 36, p. 1701349, 2017, doi: 10.1002/smll.201701349.
33 K. Yamada *et al.*, 'Ultrathin Bismuth Film on 1T-TaS2: Structural Transition and Charge-Density-Wave Proximity Effect', *Nano Lett.*, vol. 18, no. 5, pp. 3235–3240, May 2018, doi: 10.1021/acs.nanolett.8b01003.
34 P. Kumar, J. Singh, and A. C. Pandey, 'Rational low temperature synthesis and structural investigations of ultrathin bismuth nanosheets', *RSC Adv.*, vol. 3, no. 7, pp. 2313–2317, Jan. 2013, doi: 10.1039/C2RA21907G.
35 Z. Yang, Z. Wu, Y. Lyu, and J. Hao, 'Centimeter-scale growth of two-dimensional layered high-mobility bismuth films by pulsed laser deposition', *InfoMat*, vol. 1, no. 1, pp. 98–107, 2019, doi: 10.1002/inf2.12001.
36 E. Aktürk, O. Ü. Aktürk, and S. Ciraci, 'Single and bilayer bismuthene: Stability at high temperature and mechanical and electronic properties', *Phys. Rev. B*, vol. 94, no. 1, p. 014115, Jul. 2016, doi: 10.1103/PhysRevB.94.014115.
37 S. Zhang *et al.*, 'Semiconducting Group 15 Monolayers: A Broad Range of Band Gaps and High Carrier Mobilities', *Angewandte Chemie International Edition*, vol. 55, no. 5, pp. 1666–1669, 2016, doi: 10.1002/anie.201507568.
38 H. Iwasaki and T. Kikegawa, 'Structural Systematics of the High-Pressure Phases of Phosphorus, Arsenic, Antimony and Bismuth', *Acta Cryst B*, vol. 53, no. 3, Art. no. 3, Jun. 1997, doi: 10.1107/S0108768196015479.
39 T. Nagao *et al.*, 'Nanofilm allotrope and phase transformation of ultrathin Bi film on Si(111)-7x7', *Phys Rev Lett*, vol. 93, no. 10, p. 105501, Sep. 2004, doi: 10.1103/PhysRevLett.93.105501.
40 X. Liu *et al.*, 'Advances of 2D bismuth in energy sciences', *Chem. Soc. Rev.*, vol. 49, no. 1, pp. 263–285, Jan. 2020, doi: 10.1039/C9CS00551J.
41 A. Crepaldi, C. Tournier-Colletta, M. Pivetta, G. Autès, F. Patthey, H. Brune, O. V. Yazyev, and M. Grioni, Structural and electronic properties of the Bi/Au(110)–1×4 surface, Phys. Rev. B 2013, 88, 195433.
42 J. H. Jeon et al., *Surf. Sci.* 2009, 603, 145
43, N. Kawakami et al., *Phys. Rev. B* 2017, 96, 205402.

44 Hricovini, K.; Richter, M. C.; Heckmann, O.; Nicolaï, L.; Mariot, J.-M.; Minár, J. Topological Electronic Structure and Rashba Effect in Bi Thin Layers: Theoretical Predictions and Experiments. J. Phys. Condens. Matter 2019, 31, 283001. https://doi.org/10.1088/1361-648X/ab1529.
45 G. Kresse, J. Furthmüller, Phys. Rev. B, **1996,** 54, 11169−11186.
46 G. Kresse, J. Furthmüller, Comput. Mater. Sci., **1996**, 6, 15−50.
47 G. Kresse, J. Hafner, Phys. Rev. B, **1993**, 47, 558−561.
48 P. E. Blöchl, , Phys. Rev. B, **1994**, 50, 17953−17979.
49 G. Kresse, D. Joubert, Phys. Rev. B, **1999**, 59, 1758−1775.
50 J. Klimeš, D. R. Bowler, A. Michaelides, J. Phys.: Condens. Matter, **2010**, 22, 022201.
51 J. Klimeš, D. R. Bowler, A. Michaelides, Phys. Rev. B, **2011**, 83, 195131.
52 W. Malone, J. Matos, A. Kara, Surf. Sci., **2018**, 669, 121–129.
53 J. Matos, H. Yildirim, A. Kara, J. Phys. Chem. C, **2015**, 119 1886−1897.
54 H. Yildirim, A. Kara, J. Phys. Chem. C, **2013**, 117, 2893−2902.
55 Tersoff, J., & Hamann, D. R. “Theory of the scanning tunneling microscope”, Phys. Rev. B, 1985, 31, 805.
57 www.p4vasp.at.
56 Hara, M.; Nagahara, Y.; Inukai, J.; Yoshimoto, S.; Itaya, K. In Situ STM Study of Underpotential Deposition of Bismuth on Au(1 1 0) in Perchloric Acid Solution. Electrochimica Acta 2006, 51, 2327–2332. https://doi.org/10.1016/j.electacta.2005.01.067.